JOURNAL OF CATALYSIS 54, 183–196 (1978)

Laser Raman Study of Benzene Adsorption on Alkali Metal X and Y Zeolites

J. J. FREEMAN AND M. L. UNLAND

Corporate Research Laboratories, Monsanto Company, 800 North Lindbergh Boulevard, St. Louis, Missouri 63166

Received December 5, 1977; revised April 20, 1978

Shifts in the laser Raman spectrum of the ring breathing mode of adsorbed benzene are used to probe the electrostatic fields within the supercage of alkali metal-exchanged X and Y zeolites. It is concluded that the excess cations in X versus Y zeolites result in higher fields at the aromatic nucleus of initially adsorbed benzene. Further increases in field are caused by crowding in the supercage as the size of the cation increases. Increased benzene loading causes the frequency of the Raman band to approach that of the liquid state. These trends are related to selectivity sequences observed when these materials are used as catalysts for the alkylation of toluene with methanol to give styrene and ethylbenzene.

INTRODUCTION

There are reports in the open literature (*1–3*) of selective alkylation of toluene with methanol or formaldehyde to form styrene and ethylbenzene. The preferred catalysts for this reaction are alkali metal-exchanged X-type zeolites with Cs and Rb forms being particularly selective. Since it appeared that this might be a useful route to styrene, an investigation of this reaction was carried out in our laboratory where it was discovered that addition of borate to a zeolite catalyst (*4*) gave somewhat improved styrene yields (see Fig. 1). Questions then arose as to the nature of the borate species, its location in the catalyst, and its function during reaction. In an attempt to answer these questions, we have studied the interaction of the simplest aromatic, benzene, with various zeolites as a function of loading by both uv diffuse reflectance spectroscopy (*5*) and laser Raman spectroscopy. From the diffuse reflectance work we found evidence of π-electron interaction with the cations in the supercage and for multiple adsorption sites within the supercage. Differences in band position between X- and Y-type zeolites were also noted. The laser Raman study described here was undertaken to obtain more detailed information on the mechanism of interaction. This was accomplished through a study of the perturbations of the ring breathing mode of benzene adsorbed in these same zeolites.

METHODS

Catalyst samples were prepared starting from powdered, binderless Na forms of zeolite X (SK20) and Y (SK40) from Linde. X-Ray diffraction patterns of these materials indicated pure X- and Y-type zeolites with unit cell constants of 24.94 $\pm$ 0.02 and 24.65 $\pm$ 0.02 Å, respectively. Carbonate fusion and acid digestion of the sample, followed by spectroscopic analysis,

0021-9517/78/0542-0183$02.00/0

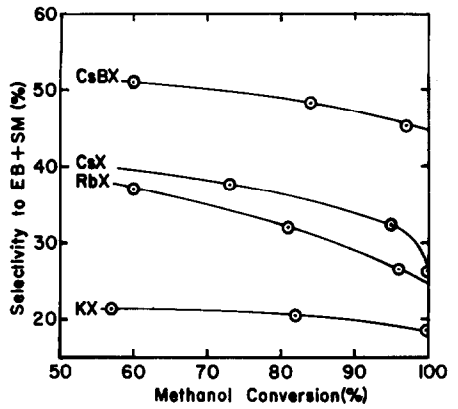

FIG. 1. Selectivity to styrene and ethylbenzene versus conversion of CH_3OH for various zeolites in the alkylation of toluene with CH_3OH.

after excitation in an inductively coupled argon plasma, gave SiO_2/Al_2O_3 mole ratios of 2.52 and 4.95 for SK20 and SK40, respectively. Unit cell constants were not significantly changed by exchange of the Na^+ with other alkali metal cations. The various cations were exchanged into the zeolites at room temperature using 0.5 *M* solutions of the respective hydroxides. Addition of borate was accomplished by adding H_3BO_3 to the hydroxide solution until a pH of 10.0 was reached. The extent of cation exchange was determined by atomic absorption analysis of the acid-digested solid.

Reactor data shown in Fig. 1 were obtained by passing vaporized toluene and methanol at a mole ratio of 5.2/1.0 over a 10-cm^3 bed of 8 × 30-mesh catalyst. The gas hourly space velocity was 950 hr^{-1} and effluent analysis was recorded at catalyst temperatures of 450, 430, and 410°C.

Zeolite samples prepared for spectroscopic studies were subjected to especial pretreatment so as to minimize laser-induced fluorescence during Raman measurements. This problem has been reviewed in detail by a number of authors (*6–10*). The method we have evolved for eliminating fluorescence arising from organic impurities on the adsorbent is based on that presented by Egerton and co-workers (*10*) and is as follows: Zeolite, 0.5 g, was subjected to vacuum dehydration at 420°C for 2 hr. While maintaining temperatures 100 Torr of O_2 was introduced into the cell and held for 30 min. The sample wa- evacuated for another 30 min while main, taining temperature and then was allowed to cool to room temperature. Greaseless O-ring seal stopcocks were used throughout the vacuum system. In spite of these precautions, sample fluorescence would occa- aionally exceed acceptable levels.

In order to bring sample fluorescence down to acceptable low levels consistently, it was found necessary to install a liquid nitrogen-cooled trap filled with activated molecular sieves in the vacuum line between the oil diffusion pump and the sample. It was observed that the effectiveness of these measures in preventing the formation of fluorescent impurities could be readily monitored by irradiating the activated sample with a simple 15-W ultraviolet mineral lamp. Visibly detectable fluorescence observed with this lamp was evidence that sample fluorescence during subsequent Raman studies would be intense enough to prevent recording of the vibrational spectrum of adsorbed benzene.[1] Weight losses on dehydration were in the range of 15 to 25%, depending on the cation in the zeolite. After dehydration, the samples were dosed with various amounts of thiophene-free benzene (Fisher) vapor at room temperature. The amount adsorbed was determined by weight difference on the same Mettler single-pan balance (±0.0002 g). It is felt that ±2 mg/g of dehydrated zeolite is a reasonable estimate of uncertainty in the benzene loadings quoted later. The maximum loading for each sample was

[1] We are indebted to Dr. P. J. Hendra, The University, Southampton, England for his suggestions on using liquid nitrogen-cooled molecular sieves for reducing sample fluorescence to acceptable levels.

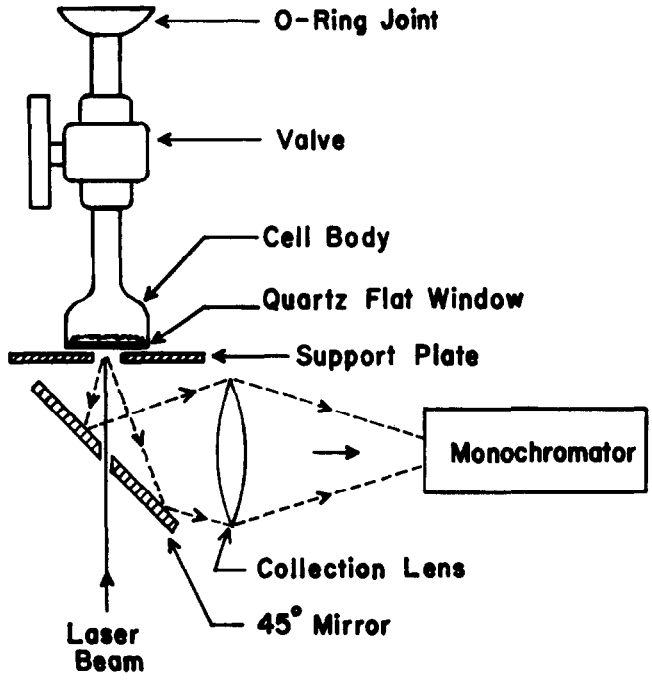

FIG. 2. Sample cell and light collection optics.

obtained by equilibration with 45 Torr of benzene.

Raman spectra were acquired with a Spex Industries Ramalog-5 spectrometer using a Coherent Radiation CR-3 argon ion laser. The laser was adjusted to yield ca. 100 mW of 19,430 cm^{-1} (514.5 nm) radiation at the sample surface. Argon plasma lines were eliminated from the laser light with a Claassen filter–100-μm slit combination. The incident beam was focused on the surface of the powdered sample and 180° backscattering collection optics were used (see Fig. 2). Scattered light was centered and focused on the entrance slit and then dispersed using the Spex 1401 double monochromator system fitted with 1800 lines/mm holographic gratings.

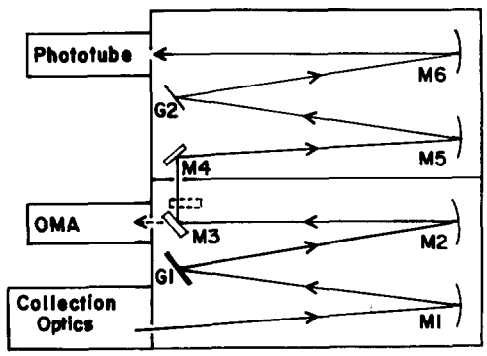

FIG. 3. Position of optical multichannel analyzer (OMA) in the optical path of the Spex 1401 double monochromator.

Signals were detected and processed either by photon counting or through the use of an optical multichannel analyzer (see Fig. 3). In photon counting detection, a thermoelectrically cooled RCA31034C phototube was employed. The alternate signal detection scheme involved the use of an optical multichannel analyzer (OMA). The particular unit used in this study is a PARC (Princeton Applied Research Corp.) 1205I ISIT tube, a gateable image intensifier coupled to a silicon-intensified target camera, which is controlled with a PARC 1205A OMA console. The ISIT detector tube was mounted at the exit port of the

first monochromator of the Spex 1401 double monochromator. The Raman radiation could be directed to either the phototube or the OMA tube by positioning of the kinematically mounted swing-a-way mirror M3 as shown in Fig. 3. The entrance and exit slits of the spectrometer were set to yield a resolution of ≤ 2 cm^{-1} at either detector. When the OMA system was in use, a 514.5-nm laser line rejection filter (Special Optics, Little Falls, N. J., No. 9-4225-514.5) was placed at the entrance slit of the spectrometer. The use of this filter was found to be an absolute necessity for preventing the OMA target face from being flooded with zero-order stray radiation. This stray radiation was found to be quite intense during investigation of powdered solid samples illuminated in 180° backscattering mode.

A Nicolet Instrument Corp. NIC-80 data processor was interfaced to the Spex digital control unit and photometric unit. The data processor was used to remotely control the spectrometer for purposes of improving signal to noise ratio through multiple scan-time averaging technique. Data were generally collected at intervals of ca. 1 cm^{-1}. Data from the PARC OMA unit were also transferred to the NIC-80 unit for purposes of frequency calculation, data comparison, plotting, or storage on a floppy disk system for later reference. The absolute accuracy of the optical system was estimated to be within ± 1 cm^{-1} based on measurements of either the emission lines of an argon gas discharge tube or the published values of the Raman lines of liquid benzene.

RESULTS

Figure 1 shows typical selectivity versus conversion curves for alkali–metal cation-exchanged type X zeolites as catalysts in the toluene plus methanol reaction. As mentioned earlier, CsX and RbX are preferred over KX catalysts, and the

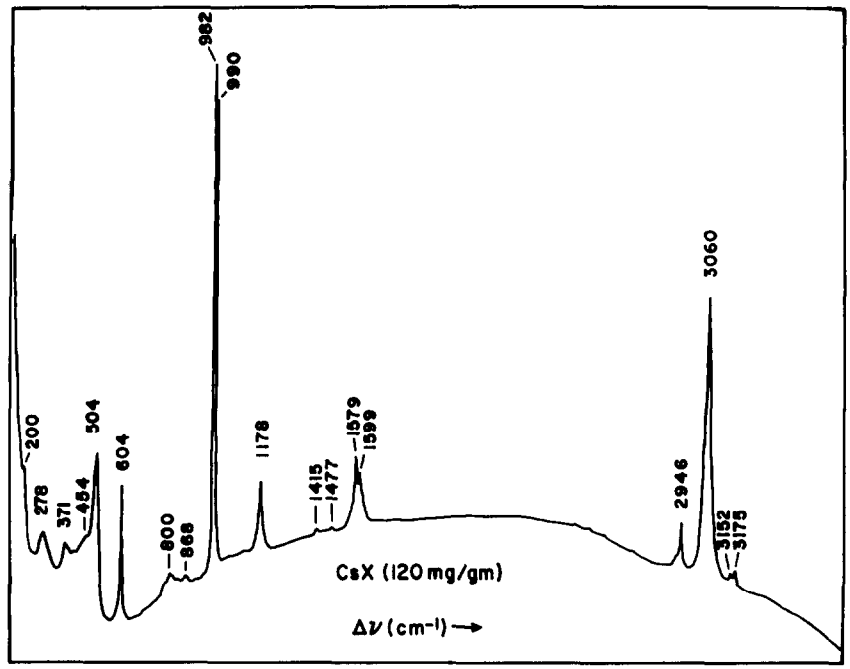

FIG. 4. Laser Raman spectrum of benzene on CsX at 120 mg/g.

TABLE 1

Raman Bands of Liquid Benzene and Benzene Adsorbed on X Zeolites

Assignment[a]			Frequency (cm^{-1})				
Symmetry	Wilson no.	Description	Liquid benzene	NaX (246 mg of ϕH/g)	CsX (42 mg of ϕH/g)	CsX (120 mg of ϕH/g)	CsBX (146 mg of ϕH/g)
e_{2g}	6a, 6b	Ring deformation	606	607 (+1)[b]	604 (−2)	604 (−2)	606 (0)
—	—	?	801	—	792 (−9)	800 (−1)	792 (−9)
e_{1g}	10a, 10b	CH out-of-plane deformation	848	—	—	868 (+20)	840 (−8)
a_{1g}	1	Ring breathing	992	989 (−3)	981 (−11)	982 (−10) 990 (−2)	984 (−8) 991 (−1)
e_{2g}	9a, 9b	CH deformation	1174	1180 (+6)	1189 (+15)	1178 (+4)	1184 (+10)
—	—	Fermi resonance of $\nu_{6a,6b}$ and ν_1	1585	1583 (−2)	1576 (−9)	1579 (−6)	1581 (−4)
			1606	1601 (−5)	1593 (−13)	1599 (−7)	1596 (−10)
—	—	—	2927	—	2933 (+6)	—	2931 (+4)
—	—	—	2947	2948 (+1)	2951 (+4)	2946 (−1)	2950 (+3)
a_{1g}	2	CH stretch	3060	3064 (+4)	3038 (−22)	3060 (0)	3042 (−18) 3061 (+1)

[a] Dollish, F. R., Fateley, W. G., and Bentley, F. F., "Characteristic Raman Frequencies of Organic Compounds," pp. 162–181. Wiley, New York, 1975.

[b] Numbers in parentheses are shifts in frequency (per centimeter) relative to liquid benzene spectrum.

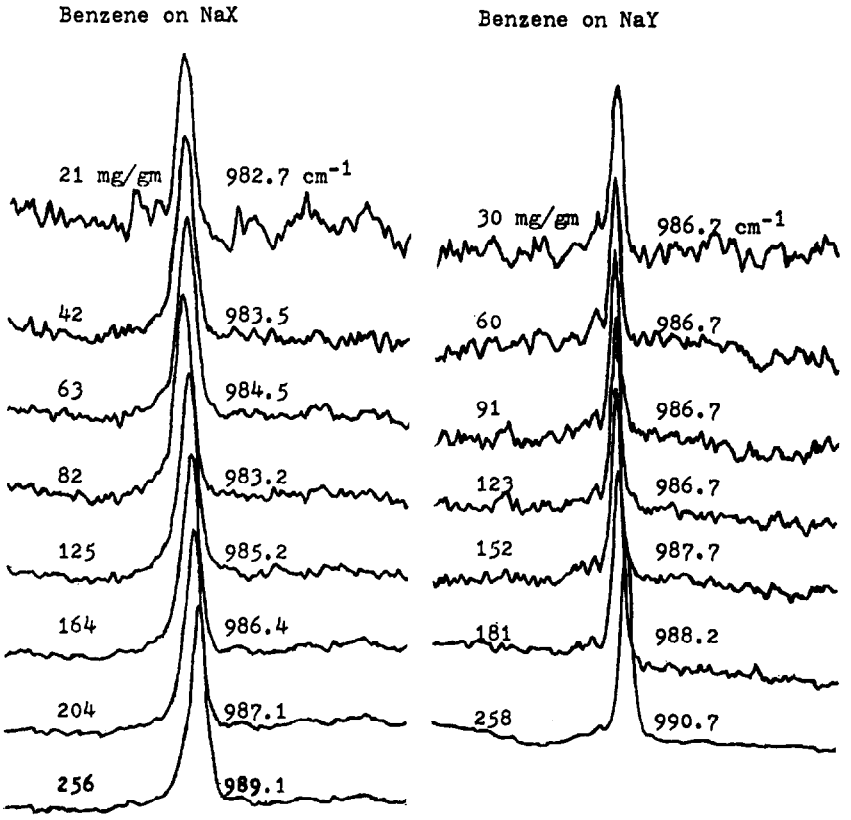

FIG. 5. Breathing mode of benzene as a function of loading on NaX and NaY.

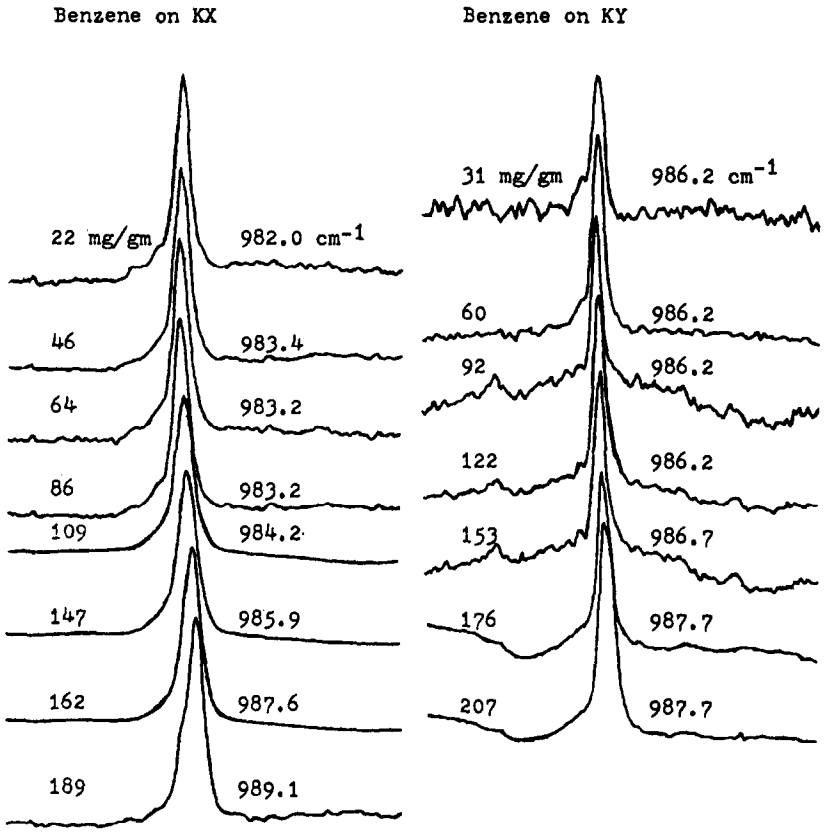

FIG. 6. Breathing mode of benzene as a function of loading on KX and KY.

borate-promoted catalyst, CsBX, is favored above all.

Figure 4 is the complete laser Raman spectrum of benzene adsorbed on a CsX sample at a loading of 120 mg/g of dehydrated sample. The most prominent bands are the ring breathing mode at $\sim$990 cm^{-1} and the CH stretch at 3060 cm^{-1}. The only readily observable band due to the support is at 504 cm^{-1}. Table 1 contains partial assignments of the bands shown in Fig. 4, as well as data on liquid benzene and benzene adsorbed on some other metal ion-exchanged X zeolites. Notice that, at higher loadings of benzene on CsX and CsBX, the ring breathing mode, ν_1, is actually a doublet. Also, on adsorption of benzene, the ring breathing and in-plane CH stretching modes are generally shifted to lower wavenumber, while out-of-plane and deformation modes are shifted to higher wavenumbers with respect to liquid benzene. As the loading of benzene increases, the Raman spectrum of the adsorbed molecules approaches that of the liquid state.

Because of the interesting splitting observed in the ν_1 band at high benzene loading on CsX and because our earlier diffuse reflectance study suggested the possibility of multiple adsorption sites in the more crowded supercages, this Raman band was studied in some detail over a series of zeolites. Accordingly, Figs. 5–8 show results using the OMA system described earlier. Due to the high variability in overall Raman scattering intensity on going from sample to sample, the spectra shown in these figures have all been normalized to the same arbitrary intensity value for the peak maximum.

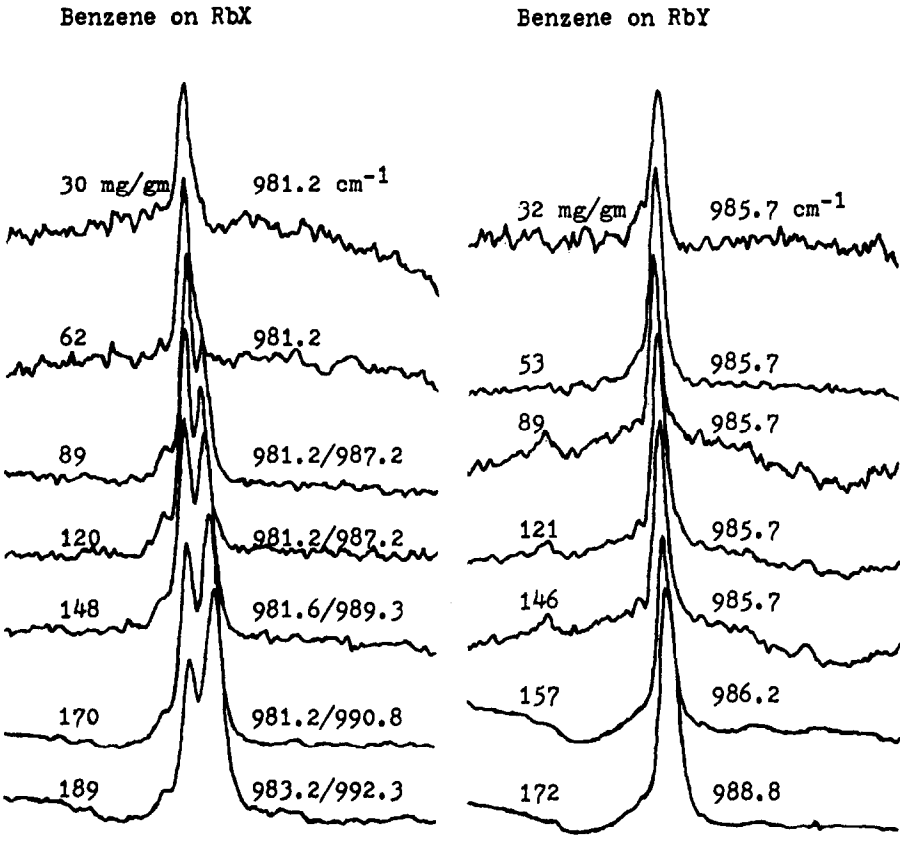

FIG. 7. Breathing mode of benzene as a function of loading on RbX and RbY.

The spectra shown in these figures dramatically exhibit the effect of loading, cation, and cation distribution (i.e., X versus Y zeolites). Notice that the splitting phenomenon is greatest with the largest cations and for type X zeolite which has the larger number of cations in the supercage (*11*).

Figures 9 and 10 clearly show a number of important trends in the data. First, at low loadings the frequency of the ring breathing mode is clearly shifted toward lower energies relative to the liquid phase. Second, as the loading on a given support is increased, the frequency of the band increases smoothly toward the liquid value of 992 cm^{-1}. Third, in the case of cesium- and rubidium-exchanged supports, a second distinct adsorption site for benzene becomes occupied. The frequency of the band in this second site continues to increase toward the liquid value as the loading increases. And, last, for low loadings the band position on Y supports is closer to the liquid value than is the band position for adsorption on X-type supports.

We have used the data in these figures to estimate, by interpolation, the band position for weight loadings corresponding to the adsorption of one molecule of benzene per supercage. These data are presented in Table 2. This table clearly demonstrates that at low loadings the Raman band is more strongly perturbed by adsorption on X than on Y zeolites.

Finally, in Fig. 11 we have constructed a plot of the position of the π–π^* electronic band of benzene as determined by diffuse reflectance spectroscopy (*5*) versus the position of the Raman band. All data have

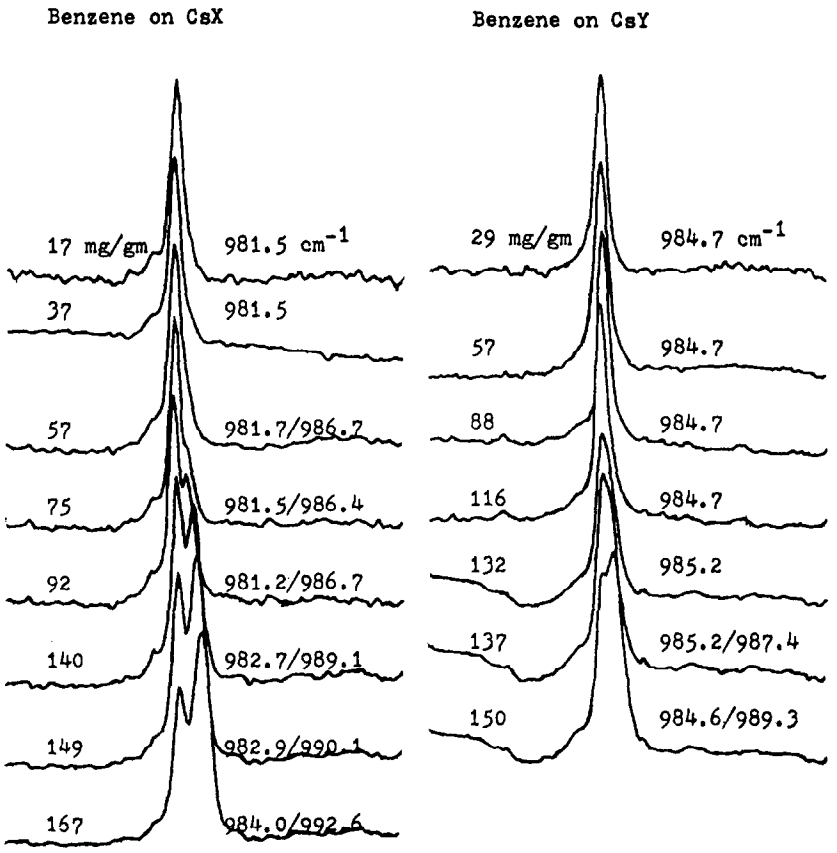

FIG. 8. Breathing mode of benzene as a function of loading on CsX and CsY.

been interpolated to a loading corresponding to the adsorption of one molecule of benzene per supercage on X-type zeolites. This plot clearly points out a direct correlation between perturbations of the π-electron structure of adsorbed benzene and the lowering in energy of the Raman active ring breathing band.

DISCUSSION

Our previous studies on the electronic spectrum of benzene adsorbed on zeolites (*5*) showed that the positions of the vibronic band maxima were dependent on both the degree of surface area coverage and the nature of the metal ion exchanged within the zeolite cage. We deduced from these results that the adsorption process involves electrostatic interaction between the π-electron system of benzene and the zeolite cage. The ultraviolet diffuse reflectance data upon which these conclusions were based did not exhibit sufficient resolution to permit detailed conclusions to be made on the exact geometry of the adsorption mechanism. The perturbations of the vibrational spectrum measured by either Raman scattering or infrared adsorption should, however, provide the additional information and resolution not obtainable in the diffuse reflectance experiments.

Earlier studies on the Raman spectrum of adsorbed benzene (*6*, *7*, *12*) did not appear to bear out the above hope. The authors found that, while Raman band intensities were altered upon adsorption, there were no significant differences between the Raman band positions of liquid and

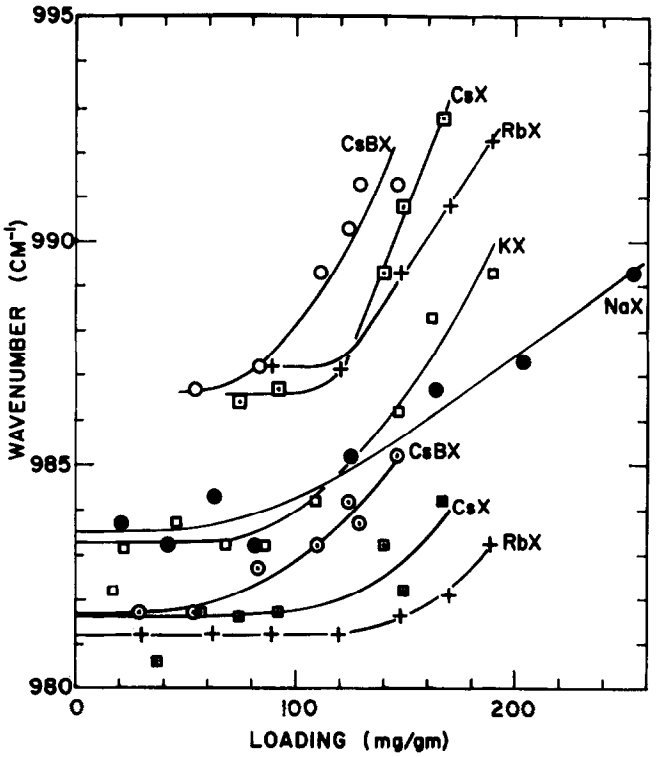

FIG. 9. Comparison of breathing mode shifts for benzene (liquid = 992 cm^{-1}) on X-type zeolites.

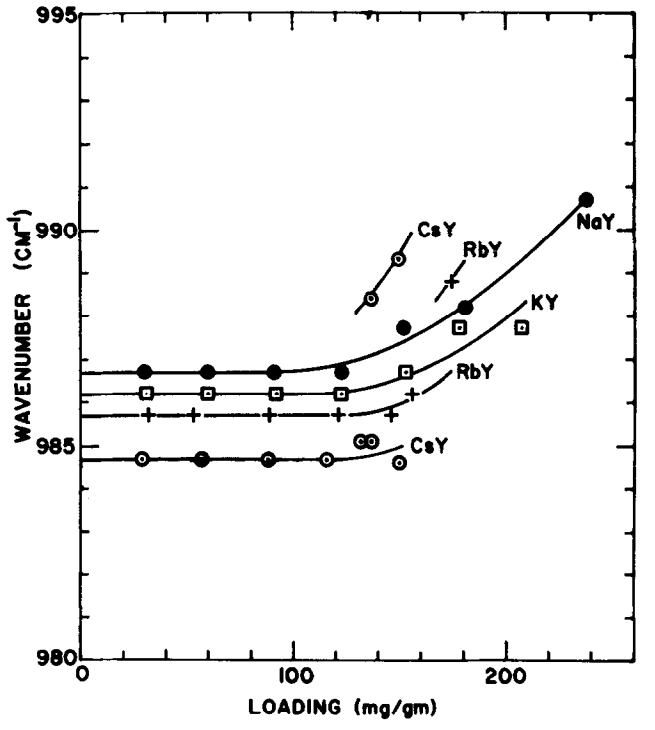

FIG. 10. Comparison of breathing mode shifts for benzene (liquid = 992 cm^{-1}) on Y-type zeolites.

TABLE 2

Sample Properties and Position of ν_1 Band of Adsorbed Benzene at One Molecule per Supercage

Sample	Exchange[a] (%)	Density[b] (g/cm³)	Loading[c] (mg/g)	Frequency (cm^{-1})	$\Delta\nu$[d] (cm^{-1})
NaX	100	1.44	46.5	983.5	−8.3
KX	86	1.57	42.5	983.3	−8.5
RbX	62	1.80	37.0	981.2	−10.6
CsX	52	1.97	34.0	981.6	−10.2
CsBX	(52)	1.97	34.0	981.7	−10.1
NaY	100	1.40	49.0	986.7	−5.1
KY	93	1.49	46.0	986.2	−5.6
RbY	67	1.66	41.2	985.7	−6.1
CsY	55	1.77	38.7	984.7	−7.1

[a] Atomic absorption analysis of zeolite (assumed for CsBX).
[b] Calculation based on dehydrated formulas. X = $Na_{86}[(AlO_2)_{86}(SiO_2)_{106}]$. Y = $Na_{56}[(AlO_2)_{56}(SiO_2)_{136}]$.
[c] Milligrams of C_6H_6 adsorbed per gram of dehydrated sample.
[d] Shift of ν_1 band of C_6H_6 from its liquid value taken as 991.8 cm^{-1}.

adsorbed benzene. A review of our data presented in Fig. 1 indicates that this is indeed the case at high benzene coverages. At lower benzene coverages, however, our data show that significant differences do occur. The data in Table 1 indicate that vibrations primarily dependent upon the strength of the carbon–carbon π-electron bond, such as the a_{1g} (ν_1) ring breathing mode and the C=C stretch at 1585 and 1606 cm^{-1}, are lowered upon adsorption. On the other hand, out-of-plane vibrations such as e_{2g} ($\nu_{9a,b}$) are increased in frequency upon adsorption. These trends in the Raman data match those observed by Angell and Howell (*13*) in their ir studies of benzene adsorbed on zeolites. These data lend credence to an adsorption mechanism which weakens the π-electron bond of the aromatic ring while simultaneously locking the ring into a fixed configuration which does not favor out-of-plane vibrations, i.e., the benzene ring becomes locked on the surface or within the zeolite cage. This picture is supported by recent NMR studies on adsorbed aromatics on zeolites (*14–18*). In one ^{13}C-NMR study (*14*) on adsorbed ethylbenzene, the ethyl group was found to rotate freely while the aromatic portion of the molecule exhibited severely restricted rotational freedom. Similar NMR studies on adsorbed benzene (*18*) showed that at low coverage the benzene molecule exhibited significantly lower mobility.

Additional details of the exact nature of the adsorption site can be obtained from a detailed consideration of the structure of the zeolite supercage. According to examples given by Breck (*11*), a dehydrated NaX sample will have 4.0 of the 5.5 Na^+ cations in each supercage fixed at site II locations. This leaves 1.5 Na^+ cations per

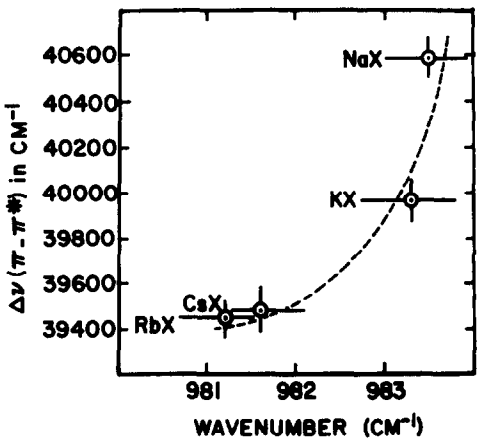

FIG. 11. Correlation of diffuse reflection uv and laser Raman results for benzene adsorption at one molecule per supercage on NaX, KX, RbX, and CsX zeolites.

supercage which are less firmly attached to the wall in other locations such as site III. On the other hand, a dehydrated NaY sample will only have ~3.75 Na^+ cations in the supercage, and it is probable that these are attached at site II. In other words, on the average, a dehydrated NaX sample will have 1.5–2.0 Na^+ ions in its supercage which are not firmly attached to site II and which are not present in a dehydrated NaY sample.

It is believed that most of the differences between X- and Y-type zeolites observed in Figs. 9 and 10 can be explained on the basis of these additional, loosely held cations present in X- but not in Y-type supercages.

It seems reasonable to propose that the first molecule of benzene to enter the supercage of an X-type zeolite complexes with a relatively exposed site III cation and is more strongly perturbed by it than are later molecules which complex with site II cations. Then, in order to rationalize the observed splitting on CsX and RbX, one might postulate that, for the larger Cs^+ and Rb^+ cations, sites II and III are energetically distinct, whereas, for the smaller Na^+ and K^+ cations, sites II and III are more nearly equivalent. The excess of cations in type X supercages and their more random location on the walls may also help explain the larger amount of scatter in Fig. 9 as opposed to the more regular nature of the data in Fig. 10. On the basis of approach to the liquid state with loading, the superage of the CsBX catalyst appears to be more crowded than the rest of the samples in Fig. 9. This conclusion is supported by the fact that, at a pressure-to-saturated vapor pressure ratio of 0.5, CsBX adsorbed less benzene than CsX (146 versus 167 mg/g of dehydrated sample). However, at very low loading, the perturbation of the ring breathing mode of benzene on CsBX and CsX was the same. It is also significant that, at low loading, the perturbation of the benzene is larger (farther from the liquid state) for X-type zeolites compared to the same cation form of Y zeolite. It is interesting that, for the borate-modified CsX catalyst (see Fig. 9), the first benzene molecule adsorbed into the supercage apparently is not affected by the presence of the borate. It is only the second or third molecule which is affected by the more crowded condition due to the presence of the borate.

Another way of explaining the cation effect and the difference between X and Y zeolites is to propose that, because of the excess of cations in X versus Y, the first benzene molecule is adsorbed in a position where it is in close contact with at least two cations. In this case, there would be a concerted perturbation of the electrons in benzene due to two positive cation charges. Then, subsequent benzene molecules will probably be complexed to single cation sites and not to sites on the wall of the supercage (*15*, *16*). After about three molecules have been adsorbed, the entry of additional molecules begins to perturb those already present and, as shown by the upward trends of the curves in Figs. 9 and 10, the nature of the adsorbed benzene begins to approach the liquid state. The proposal to a two-site adsorption mechanism would seem to be supported by other Raman work (*12*) and by analogy with the structure of the naphthalene/$SbCl_3$ complex (*19*).

It is not clear which mechanism for adsorption of the first benzene molecule in an X-type zeolite supercage is correct, although the ^{13}C-NMR results in our laboratories (*14*) on ethylbenzene adsorption showed that there is little rotational freedom in the CsX supercage which tends to support a two-point adsorption picture. The same conclusion results from a study of models of the supercage with Na^+ cations replaced by Cs^+ cations. Dempsey (*20*) has calculated the electrostatic fields (E) at various distances from site II and site III cation surfaces in NaX and NaY

zeolites and has found that E (X site III) > E (Y site II) > E (X site II). If we take the frequency of the ν_1 mode of benzene at $P/P_0 = 0.5$ on NaX as characteristic of X site II, and values from Table 2 at one molecule per supercage as characteristic of adsorption at X site III and Y site II, and plot these numbers against Dempsey's values for field strength at a distance of 1 Å from these sites, the correlation found in Fig. 12 results. Thus, the higher the field strength at a given site, the more perturbation from the liquid state one sees in the ring breathing mode of the initial molecule of adsorbed benzene. Also, if we take other values of ν_1 from Table 2 and place them on the line in Fig. 12, one concludes that the presence of larger cations in the supercage also results in a higher field strength at the benzene molecule. Since the larger radii of Cs^+ and Rb^+ should result in lower, not higher, field strengths at a given point, one may again resort to a concerted interaction by two or more cations within the supercage to explain the apparent higher field strengths at the benzene molecule and the observed shifts in the breathing mode.

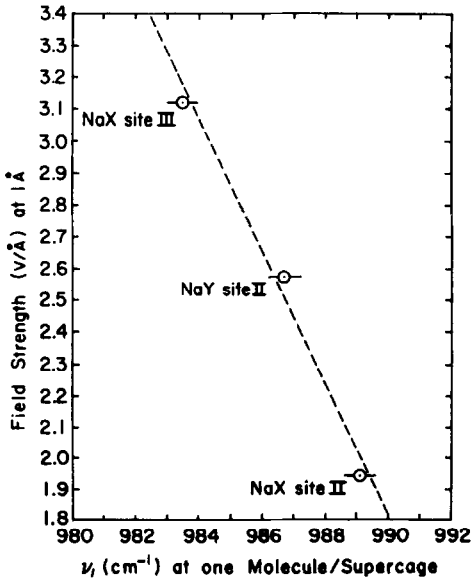

FIG. 12. Comparison of calculated electrostatic field (*20*) at 1 Å from the surface of various sites with the frequency of the ring breathing mode of adsorbed benzene.

TABLE 3

Comparison of Trends in Electronic and Vibrational Spectra as a Function of Changes in Cation Size, SiO_2/Al_2O_3 Ratio, and Benzene Loading.

System perturbation	Result (at one C_6H_6/supercage)	
	Electronic (π–π^*)	Vibrational (ν_1)
Increase cation radius ($Na^+ \rightarrow Cs^+$)	Red shift[a]	Red shift
Increase SiO_2/Al_2O_3(X → Y)	(Blue shift)[b]	Blue shift
Increase C_6H_6 loading	Red shift	Blue shift
Increase electrostatic field at C_6H_6 (Y site II → X site III)	(Red shift)[b]	Red shift

[a] A red shift is a shift to lower wavenumber or energy.

[b] Regarded as tentative because diffuse reflectance data (*5*) were extrapolated back to one molecule per supercage.

In Fig. 11 it was noted that there is some correlation between changes in electronic transitions (*5*) and vibrational transitions as the size of the cation in the supercage is changed. As the cation size increases in the series from Na^+ to Cs^+, both electronic and vibrational transitions are shifted to the red (i.e., lower wavenumber or energy). Table 3 summarizes these results and compares other trends as well. Except for the increase in electrostatic field, all entries in Table 3 are based on experimental observations. These results demonstrate that perturbation of the benzene molecule as it is adsorbed is affecting both electronic and vibrational energy levels. In the case of benzene loading (in Table 3), the opposite effects on electronic and vibrational transitions are attributed to benzene–benzene dispersion interactions which should strongly affect only electronic transitions.

The correlation in Fig. 12 was the basis for claiming a red shift of the ν_1 breathing mode with increase in electrostatic field and for the conclusion that such fields are stronger in the crowded Cs-containing supercage than in the Na-containing supercages. Unfortunately, data from our diffuse reflectance study (*5*) did not extend to the low coverages necessary to make conclusions regarding the electronic transition with similar confidence. Therefore, the trends in parentheses in Table 3 are somewhat tentative.

Finally, one must ask how these results relate to the observed differences in catalyst performance presented in Fig. 1 where the observed sequence of selectivity at constant conversion is NaX < KX < RbX < CsX. From Table 3 we infer that the electrostatic field at the aromatic nucleus is also increasing as one goes from Na^+ to Cs^+ in the confines of a type X supercage. One could also infer from Table 3 that the first molecule adsorbed in an X-type zeolite will experience a higher electrostatic field than one adsorbed in a Y-type supercage. It is known that X-type zeolites are preferred catalysts over Y-type zeolites for the toluene plus methanol reaction (*1*). It therefore seems consistent to interpret electronic spectroscopy, vibrational spectroscopy, and reactor results as stemming from changes in the electrostatic fields experienced by the aromatic nucleus. The necessary electrostatic fields are produced by crowding as many large monovalent cations as possible into the fixed geometry of a zeolite supercage so that simultaneous interaction of the molecule with two or more electron acceptors (cations) can occur. It was noted earlier that borate incorporated into the zeolite supercage produces an enhancement of catalyst selectivity and that the borate did not affect initial adsorption of benzene. Thus, we conclude that in the toluene plus methanol reaction the borate is acting on the methanol decomposition rather than the toluene activation portion of the reaction. The exact mechanism by which the borate alters methanol decomposition is not known, although we have some evidence (*14*) that borate inhibits the formation of formate species on the CsX catalyst.

SUMMARY

The instrumental advantages of rapid scan laser Raman spectroscopy using an optical multichannel analyzer bring real-time studies and loading studies requiring a large number of samples into the realm of possibility.

The extra unlocatable cations in alkali metal X zeolites which are not present in Y zeolites produce unique sites for activation of an aromatic nucleus through a two (or more)-point complex formation mechanism. This mechanism is believed to result in higher electrostatic fields at aromatic nuclei adsorbed in X-type zeolites containing large cations such as Cs^+ and Rb^+ and thereby helps explain the unique activity of these catalysts for the alkylation of toluene to styrene with methanol.

The laser Raman results show that the borate used as a selectivity promoter in CsX catalysts for the alkylation of toluene to styrene with methanol is located in the supercage, but is probably not directly involved in the activation of the aromatic molecule. Rather, it is believed that the selectivity enhancement is achieved by helping to control the decomposition of methanol.

ACKNOWLEDGMENTS

We wish to acknowledge Dr. G. E. Barker for the catalyst testing results and Dr. N. A. Fishel and Dr. J. F. Roth for many discussions of this work. Also, we wish to acknowledge the able technical assistance of Mr. S. D. Koban in catalyst preparation.

REFERENCES

1. Yashima, T., Sato, K., Hayasaka, T., and Hara, N., *J. Catal.* **26**, 303 (1972).
2. Sidorenko, Y. N., Galich, P. N., Gutyrya, V. S.,

Il'in, V. G., and Neimark, I. E., *Dokl. Akad. Nauk SSSR* **173**, 132 (1967).
3. Sidorenko, Y. N., and Galich, P. N., *Ukr. Khim. Zh.* **36**, 1234 (1970).
4. U. S. patent applied for.
5. Unland, M. L., and Freeman, J. J., *J. Phys. Chem.*, accepted for publication.
6. Buechler, E., and Turkevich, J., *J. Phys. Chem.* **76**, 2325 (1972).
7. Egerton, T. A., Hardin, A. H., Kozirovski, Y., and Sheppard, N., *J. Catal.* **32**, 343 (1974).
8. Egerton, T. A., and Hardin, A. H., *Catal. Rev. Sci. Eng.* 11, 1 (1975).
9. Angell, C. L., *J. Phys. Chem.* **77**, 222 (1973).
10. Egerton, T. A., *et al.*, *Canad. J. Chem.* **54**, 586 (1976).
11. Breck, D. R., "Zeolite Molecular Sieves," pp. 99–100. Wiley, New York, 1974.
12. Winde, H., *Z. Phys. Chem.* (*Leipzig*) **257**, 392 (1976).
13. Angell, C. L., and Howell, M. V., *J. Colloid Interface Sci.* **28**, 279 (1968).
14. Sefcik, M., private communication.
15. Pfeifer, H., and Geschke, D., *Z. Phys. Chem.* (*Leipzig*) **257**, 365 (1976).
16. Lechert, H., Haupt, W., and Kacirek, H., *Z. Naturforsch.* **30a**, 1207 (1975).
17. Hoffman, W. D., *Z. Phys. Chem.* (*Liepzig*) **257**, 315 (1976).
18. Borovkov, V. Yu., Hall, W. K., and Kazanski, V. B., *J. Catal.* **51**, 437 (1978).
19. Hulme, R., and Szymanski, J. T., *Acta Crystallogr. B* **25**, 753 (1969).
20. Dempsey, E., "Molecular Sieves," p. 293. Society of Chemical Industry, London, 1968.